Molecular Simulation to Investigate the Cofactor Specificity for *Pichia stipitis* Xylose Reductase

Xiao-Le Xia[1], Shan Cong[2], Xiao-Rong Weng[1], Jin-Hua Chen[1], Jing-Fang Wang[2,3,5,*] and Kuo-Chen Chou[4,5]

[1]*Key Laboratory of Industrial Biotechnology (Ministry of Education), School of Biotechnology, Jiangnan University, Wuxi 214122, China*

[2]*Key Laboratory of Systems Biomedicine of Ministry of Education, Shanghai Center for Systems Biomedicine, Shanghai Jiao Tong University, Shanghai 200240, China*

[3]*Shanghai Center for Bioinformation and Technology, Shanghai 200235, China*

[4]*Center of Excellence in Genomic Medicine Research (CEGMR), King Abdulaziz University, Jeddah, Saudi Arabia*

[5]*Gordon Life Science Institute, Belmont, Massachusetts 02478, USA*

Abstract: Xylose is one of the most abundant carbohydrates in nature, and widely used to produce bioethanol via fermentation in industry. Xylulose can produce two key enzymes: xylose reductase and xylitol dehydrogenase. Owing to the disparate cofactor specificities of xylose reductase and xylitol dehydrogenase, intracellular redox imbalance is detected during the xylose fermentation, resulting in low ethanol yields. To overcome this barrier, a common strategy is applied to artificially modify the cofactor specificity of xylose reductase. In this study, we utilized molecular simulation approaches to construct a 3D (three-dimensional) structural model for the NADP-dependent *Pichia stipitis* xylose reductase (PsXR). Based on the 3D model, the favourable binding modes for both cofactors NAD and NADP were obtained using the flexible docking procedure and molecular dynamics simulation. Structural analysis of the favourable binding modes showed that the cofactor binding site of PsXR was composed of 3 major components: a hydrophilic pocket, a hydrophobic pocket as well as a linker channel between the aforementioned two pockets. The hydrophilic pocket could recognize the nicotinamide moiety of the cofactors by hydrogen bonding networks, while the hydrophobic pocket functioned to position the adenine moiety of the cofactors by hydrophobic and π-π stacking interactions. The linker channel contained some key residues for ligand-binding; their mutation could have impact to the specificity of PsXR. Finally, it was found that any of the two single mutations, K21A and K270N, might reverse the cofactor specificity of PsXR from major NADP- to NAD-dependent, which was further confirmed by the additional experiments. Our findings may provide useful insights into the cofactor specificity of PsXR, stimulating new strategies for better designing xylose reductase and improving ethanol production in industry.

Keywords: Xylose reductase, NADP-dependence, Molecular modelling, Mutagenesis, Bioethanol production.

1. INTRODUCTION

Xylose reductase is a key enzyme to produce xylose from xylulose, which is one of the most abundant carbohydrates in nature, and also one of the fermentable carbohydrates in lignocellulosic biomass [1, 2]. Commonly as a homodimeric oxidoreductase, this enzyme is belonged to the aldo-keto reductase superfamily [3], which is composed of more than 100 members and widely distributed in organisms with some kinds of interactions with NAD and/or NADP [4]. Using NAD or NADP as a cofactor, xylose reductase functions to catalyze the reduction of xylose into xylitol in a reversible way, which is also known as an initial step in the assimilation of xylose into the glycolytic pathway [5]. Experimental evidences showed that the proteins or enzymes in the aldo-keto reductase superfamily adopt a bi-bi mechanism during their catalytic functions: binding to the cofactor first and subsequently the carbonyl substrates. In human, these enzymes can reduce the open chain forms of glucose to sorbitol, which are considered to be physiologically significant for diabetes when the blood glucose levels are elevated [6, 7].

The fermentation utilizing xylose reductases to bioethanol is also thought to have remarkable economical and industrial potential [8]. However, *Saccharomyces cerevisiae*, a most commonly used ethanol producer in industry, cannot efficiently utilize xylose reductases [9]. A major strategy to overcome this barrier in the fermentation to bioethanol is to introduce related genes involved in xylose metabolism from other organisms [10, 11]. Xylose reductase and xylitol dehydrogenase from *Pichia stipitis* (PsXD) are the major enzymes widely used in recombinant *Saccharomyces cerevisiae* strains engineered for xylose utilization in industry [12]. In such a way, xylose can be translated into xylulose by

*Address correspondence to this author at the 800 Dongchuan Road, Shanghai Center for Systems Biomedicine, Shanghai Jiao Tong University, Shanghai 200240, China; Tel: (86) 21 3420-7344; Fax: (86) 21 3420-6059; E-mail: jfwang8113@sjtu.edu.cn

1875-6638/13 $58.00+.00

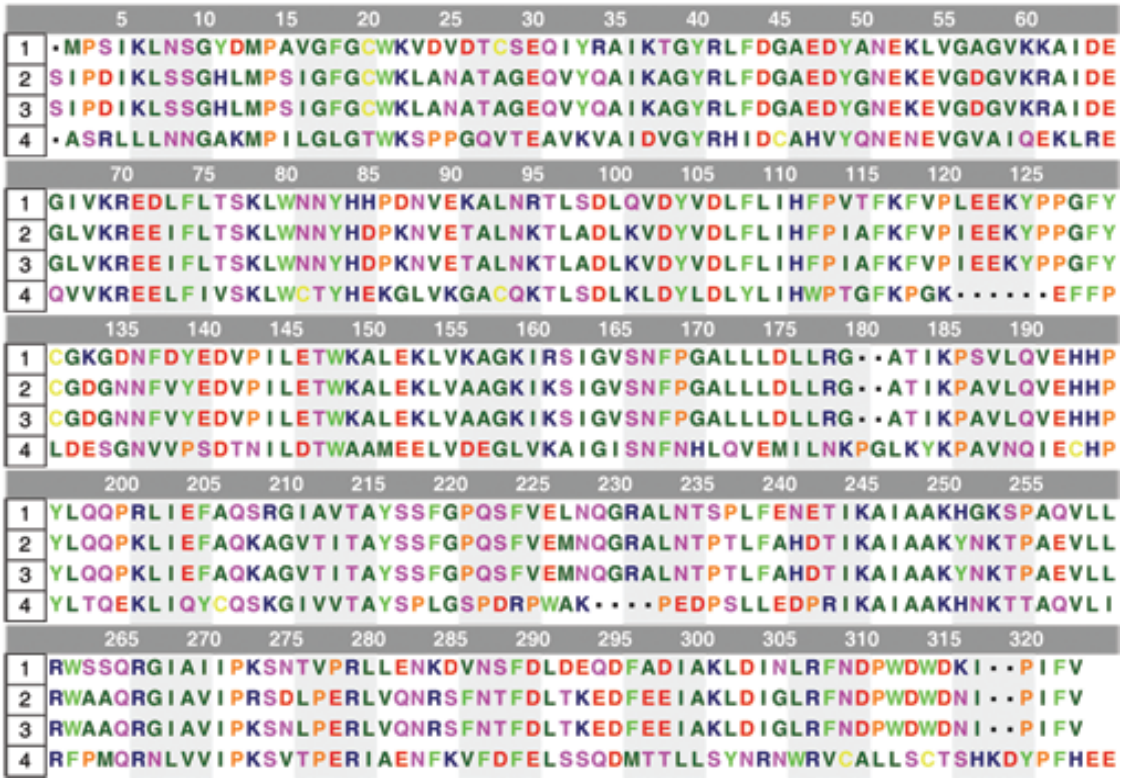

Fig. (1). The multiple sequence alignment of the target protein PsXR with its template structures. Chain 1 is the sequence of the target protein PsXR; chains 2, 3, and 4 are the sequence of its homology proteins 1sm9.pdb, 1mi3.pdb, and 1ads.pdb, respectively. The amino acids are colored according to the following 7 types: (i) acidic, red; (ii) basic, dark blue; (iii) neutral hydrophilic, pink; (iv) aliphatic, green; (v) aromatic, light green; (vi) thiol-containing, yellow; (vii) imino, organ. The sequence similarity scores of the target protein with 1sm9.pdb, 1mi3.pdb, and 1ads.pdb are 76%, 76%, and 41%, respectively. (For interpretation of the references to color in this figure legend, the reader is referred to the web version of this paper).

the sequential actions of 2 oxidoreductases: i) xylose reductase from *Pichia stipitis* (PsXR) can catalyze the reduction of xylose into xylitol with NADP as a cofactor; and ii) the product xylitol is subsequently oxidized by PsXD using NAD exclusively as a cofactor to yield xylulose. However, the disparate cofactor specificity for PsXR and PsXD will lead to an intracellular redox imbalance and low ethanol yields.

A possible strategy to deal with the intracellular redox imbalance is to artificially alter the cofactor specificity for PsXR or PsXD. Based on such idea, many good attempts have been made to alter the cofactor specificity for PsXR and PsXD using site-directed mutagenesis studies [13-18]. Most of the successful cases were only detected for PsXD, while those of PsXR were less efficacious. In the current study, we employed a series of computational tools to model the three-dimensional (3D) structure of PsXR, followed by finding a favourable binding mode of PsXR with NAD and NADP, so as to provide useful structural insights into the cofactor specificity of PsXR.

2. MATERIALS AND METHOD

2.1. Constructing 3D Structure Model for PsXR

The entire sequence of PsXR was obtained from the Protein Information Resource (PIR) database with a number of JQ1387. Multiple threading algorithms [19-22] were subsequently adopted to search for the structures in the Protein Data Bank (PDB), and finally 4 structures (1sm9.pdb, 1mi3.pdb, 1ads.pdb and 2pdm.pdb) were found to have similar folding with PsXR. Among these structure, the crystal structure of Candida tenuis xylose reductase (PDB ID 1sm9 [23]) was selected as final template due to its comparatively high sequence similarity (~76%) with the target protein. According to the template structure and multiple sequence alignment (Fig. **1**), the 3D structural model of PsXR was derived by the coordinate reconstruction approach [24] and ab initio modeling [25]. The former was used to predict the aligned region structures based on the template fragments, whereas the latter was employed to construct the unaligned region structures.

2.2. Flexible Docking Procedure

As there is no crystal structure of PsXR-NAD (or NADP) complex, we have to employ computational methods to construct a NAD or NADP binding mode for PsXR. Based on the 3D structural model of PsXR, flexible docking procedure was carried out with Monte Carlo simulated annealing to get the favourable binding modes for NAD and NADP. Before conducting the docking operations, 10,000 configurations of the structural model were randomly extracted from a short-time molecular dynamics simulation. NAD and NADP were subsequently docked into all these configurations to search for the favorable binding modes, and the best 100 modes for each configuration were taken for the further analyses.

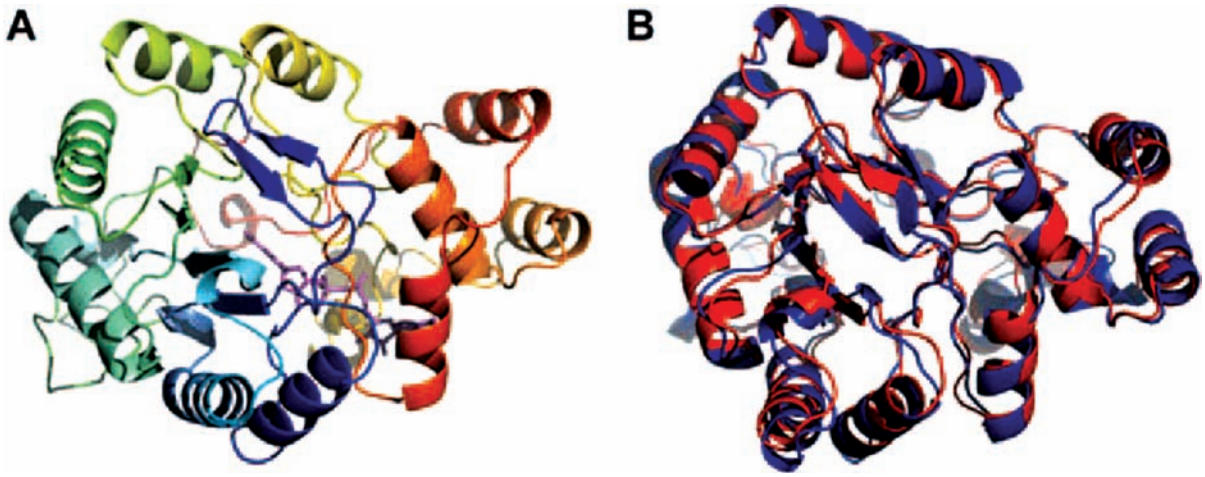

Fig. (2). Ribbon drawing to show the 3D structure of PsXR developed by the coordinate reconstruction and ab initio modeling. (A) The backbone structure of PsXR, in which the cofactor NAD is depicted with pink stick drawing. (B) A superimposition of PsXR with its template structure 1sm9.pdb, where PsXR is colored in red, while 1sm9.pdb in blue. (For interpretation of the references to color in this figure legend, the reader is referred to the web version of this paper).

2.3. Molecular Dynamics Simulation

Here the molecular dynamics simulations were performed by Amber 11 package [26] with the Amber force field parameters [27], periodic boundary conditions and NPT ensembles. Before starting the simulations, the simulation systems were solvated with explicit TIP3P waters [28] embedded in a specified simulation box. The simulation systems were subsequently subjected to the energy minimization with the steepest descents approach [29] for ~3000 steps, followed by the conjugated gradient method [30] for the next 2000 steps. Finally, 10-ns molecular dynamics simulation was performed for each simulation system at a constant template of 310 K. During the simulations, all the bonds were constrained by SHAKE algorithm [31] with a tolerance of 10^{-6} and atom velocities for start-up runs were obtained according to the Maxwell distribution at 310 K [32]. The particle mesh Ewald (PME) algorithm [33] was employed to treat electrostatic interactions with interpolation order of 4 and a grid spacing of 0.12 nanometer (nm) [34]. The van der Waals interactions were treated by using a cut-off of 12 Å [35]. The integration step was set to be 2 femtosecond (fs), and the coordinates were saved every 1 picosecond (ps).

2.4. Experimental Validation

The mutants of PsXR were constructed by PCR-based site-directed mutagenesis using a QuikChange® Site-Directed Mutagenesis Kit (Stratagene). Each mutant was verified by DNA sequencing (Sangon Biotechnology Company, Shanghai, China) and amino acid sequence alignment. The *E.coli* BL21 (DE3) harboring the expression plasmid for the His-tagged wild-type and mutated enzymes were grown at 37°C overnight in LB medium supplemented with Kanamycin. The saturated overnight cultures were diluted 100-fold into fresh LB media containing Kanamycin and grown for ~ 2 hours to a turbidity of 0.6 at 600 nm. After the addition of 1 millimol (mM) isopropyl-β-D-thiogalactopyranoside, the culture was further grown at 25°C for 4 hours to induce the expression of the proteins.

After harvested by centrifugation at 10,000 generations for 10 minutes at 4°C, the cells were resuspended in 5 milliliter (ml) of Buffer A (20 mM sodium phosphate, pH 7.4 containing 500 mM NaCl and 20 mM imidazole) and subjected to 99 pulses of sonication, 5s each with a 9s interval in an ice-water bath. After centrifugation of the cell lysate at 10,000 generations for 10 minutes to remove cell debris, the resultant supernatant was purified by an ÄKTA purifier system using a Ni^{2+}-charged 1 ml HisTrap® FF Crude column (GE Healthcare) equilibrated with Buffer A. SDS-polyacrylamide gel electrophoresis (PAGE) was carried out in 10% slab gels.

The specific activity was determined by measuring the decrease in absorbance at 340 nm at 35°C corresponding to the oxidization of NAD(P)H to NAD(P) using a spectrophotometer. The standard assay mixture contained 80 mM xylose and 100 mM NAD(P)H in 50 mM sodium phosphate buffer (pH 6.5). All reactions were started with the addition of 100 microliter (μl) of enzyme to a final volume of 3.0 ml. One unit of enzyme activity refers to 1 micromol (μm) of NAD(P)H reduced per minute. Protein concentrations were determined using absorbance at 280 nm.

3. RESULTS AND DISCUSSION

3.1. Structure Model for PsXR

It was found from the 3D structural model of PsXR (Fig. **2A**) that the enzyme folded into a $(\beta/\alpha)_8$ barrel, which has been adopted by most of xylose reductases. As sharing a comparatively high sequence similarity with the template structure, the overall structure of PsXR seemed quite like the template structure (Fig. **2B**). To validate the 3D structural model, we employed multiple algorithms to estimate the local and global model qualities and stereochemical features. The local model quality was assessed by QMEAN [36], a scoring function of a linear combination of 6 structural descriptors (Cβ interaction energy, all-atom pairwise energy, salvation energy, torsion angle energy, secondary structure, and solvent accessibility). The QMEAN score, ranging between 0 and 1 with higher value to reflect a better quality of

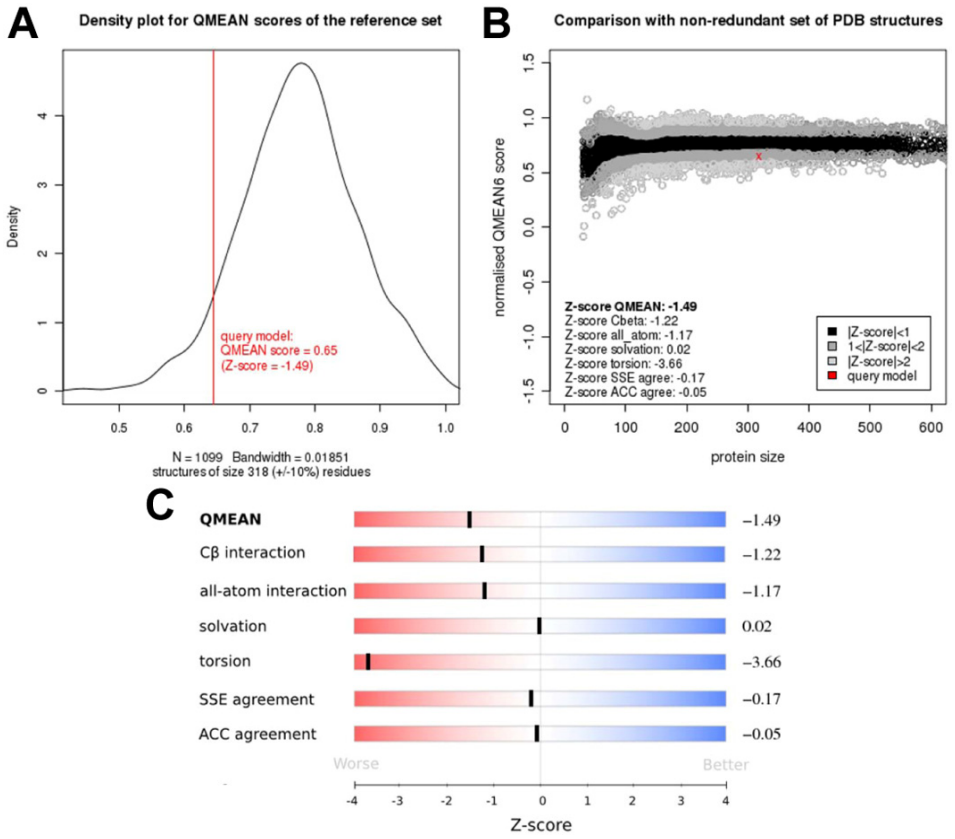

Fig. (3). The local quality for the 3D structural model of PsXR estimated by QMEAN scores. (A) The density plot of the QMEAN scores for the computational model. (B) Z-score for the computational model in comparison with the scores of the reference X-ray structures of similar size from Protein Data Bank. (C) Z-score for each QMEAN components of the computational model in comparison with the average X-ray structures.

the model, for the current model was 0.645, and the density plot of this score was shown in (Fig. **3A**). To further evaluate the absolute model quality, a Z-score of the structural model was also calculated in comparison with thoses of the reference X-ray structures of similar size from the Protein Data Bank (Fig. **3B**). For each QMEAN component, the Z-score was calculated in comparison with the average X-ray structures, in which the average score was 0 (Fig. **3C**).

The global model quality was estimated by DFIRE [37], an all-atom statistical potential based on a distance-scaled finite ideal-gas reference state to assess non-bonded atomic interactions in the protein model. DFIRE can provide pseudo energies for the computational model that reflected the quality of the model. The DFIRE score for our structural model was -427.58, indicating that the model was close to the native conformation. To further examine the stereochemical features of the structural model, we also involved Procheck [38], which indicated that 84.8% residues of the structural model were located in the core region, 10.5% in the allowed region, 2.9% in the general region, and only 1.8% in the disallowed region. For a good quality model, the residues located in the core and allowed regions should be expected to be over 90%, which is the case for our model since 84.8% + 10.5% = 95.3%. Moreover, for the main-chain residues, 98.3% of the bond lengths and 83.0% of the bond angles are within the allowed limits. All these information indicated that our computational structure of PsXR was reliable.

3.2. Favorable Binding Modes of NAD and NADP

Based on the 3D structural model of PsXR, we employed flexible docking procedure, molecular dynamics simulation and free energy calculations to get a favorable binding mode for both NAD and NADP. As sharing a similar folding structure, the cofactor binding site in PsXR could be predicted according to that of the template structure, which have been well studied and mapped out [23]. Based on the cofactor binding information of the template structure, we successfully identified the cofactor binding site in PsXR, and docked the cofactors (NAD and NADP) into the 3D structural model of PsXR (Fig. **4**).

The information of the binding pocket of a receptor to its ligand is very important for drug design, particularly for conducting mutagenesis studies [19]. In the literature, the binding pocket of a protein receptor to a ligand is usually defined by those residues that have at least one heavy atom (i.e., an atom other than hydrogen) with a distance $\leq$5 Å from a heavy atom of the ligand. The binding pocket thus found for the current cofactor looks like a dumbbell that is composed of 3 major components: a hydrophilic pocket for the nicotinamide moiety of the cofactor formed by Asp43, His110, Asn166, Gln187 as well as Tyr213; a hydrophobic pocket for the adenine moiety of the cofactor formed by Trp20, Phe216, Pro218 as well as Phe236; and a linker channel formed by Gly18, Lys77, and Ile268.

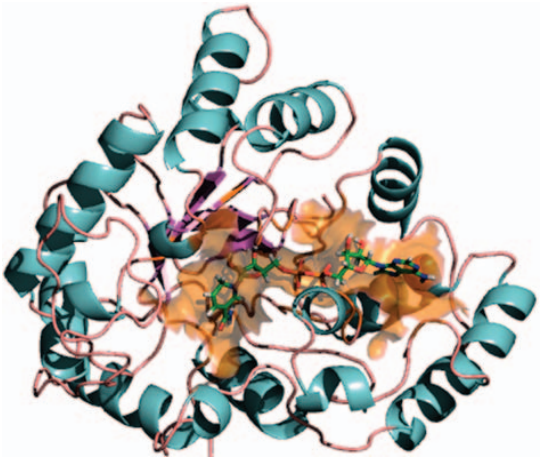

Fig. (4). Cofactor binding site in the 3D structural model of PsXR. The backbone structure of PsXR is shown in ribbon drawing with the colors based on its secondary structures. The cofactor NAD shown in stick drawing and its binding pocket is in the orange surface. The cofactor binding pocket is composed of three major parts: a hydrophilic pocket that can recognize the nicotinamide moiety of NAD; a hydrophobic pocket that can bind the adenine moiety of NAD; and a linker channel that connects the above two pockets. (For interpretation of the references to color in this figure legend, the reader is referred to the web version of this paper).

The interactions between cofactors and the residues in these components of the cofactor binding site were quite different. The residues in the hydrophilic pocket were recognizing and positioning the nicotinamide moiety of the cofactors mainly via a hydrogen bonding network (Fig. **5**). In the current case, let us define the hydrogen bond with the interaction scope that the distance between the heavy atoms of a donor and an acceptor was less than 3.5 Å and that the donor-H-acceptor angle was less than 30° [39]. For a significant hydrogen bond, the life-time should be expected to be more than 10% in all the frames involved in our simulations. The detailed information for the significant hydrogen bonds was described in Table **1**. Although both Asn166 and Gln187 could form significant hydrogen bonds to recognize the amido group of the nicotinamide moiety of the cofactors, they played different roles: Asn166 acted as a hydrogen donor, while Gln187 did as a hydrogen acceptor. The hydrogen bonds formed by Asp43 and Tyr48 functioned to position the multiple hydroxyl groups in the nicotinamide moiety of the cofactors. For the hydrophobic pocket, van der Waals interactions had major contributions to the cofactor binding. The hydrophobic residues in this pocket, such as Trp20, Pro218 as well as Phe216, could provide crucial hydrophobic interactions with the adenine moiety of the cofactors. Besides these hydrophobic interactions, Phe236 could form π-π stacking interactions with the aromatic rings in the adenine moiety, which was also considered to be essential for recognizing and positioning the adenine moiety of the cofactors. Additionally, the residues in the linker channel could provide both hydrogen bonding (i.e., Lys270) and van der Waals interactions (i.e., Ile268) to stabilize the phosphate group locating between the nicotinamide and adenine moieties of the cofactors.

3.3. Strategy for Altering the Cofactor Specificity of PsXR

To explore the cofactor specificity of PsXR, we docked both NAD and NADP into the cofactor binding site mentioned above. Due to having strong van der Waals and electrostatic interactions, the binding affinity of NADP was 1.5-fold higher than that of NAD, which also indicated the fact that PsXR was NADP specific. To alter the current cofactor

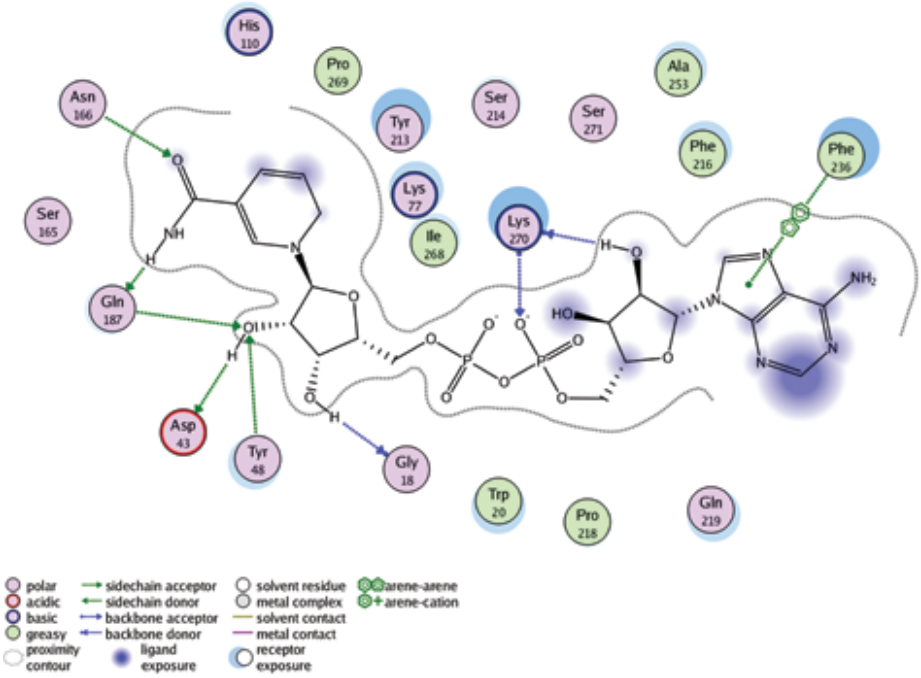

Fig. (5). A 3D diagram to show the details of the interactions between the cofactors and the residues in the active site. The interactions in the hydrophilic pocket are mainly involved with the multiple hydrogen bonding networks to position the nicotinamide moiety of the cofactors. In contrast, the hydrophobic pocket may recognize the adenine moiety of the cofactors via the π-π stacking interactions.

Table 1. The Detailed Information for the Hydrogen Bonding Interactions Formed by the Cofactors and the Residues Around their Binding Site

No.	Residues	Cofactors	Life-time	Distance/Å
1	Gly18	Nicotinamide moiety	67.4%	1.74
2	Gln187	Nicotinamide moiety	55.7%	2.79
3	Asp43	Ribose 1	52.0%	1.64
4	Gln187	Nicotinamide moiety	34.3%	1.91
5	Tyr48	Ribose 2	27.6%	2.86
6	Tyr48	Ribose 2	27.6%	2.86
7	Asn166	Nicotinamide moiety	20.9%	3.04
8	Lys270	Adenine moiety	15.3%	2.93
9	Lys270	Phosphate group	14.9%	1.48

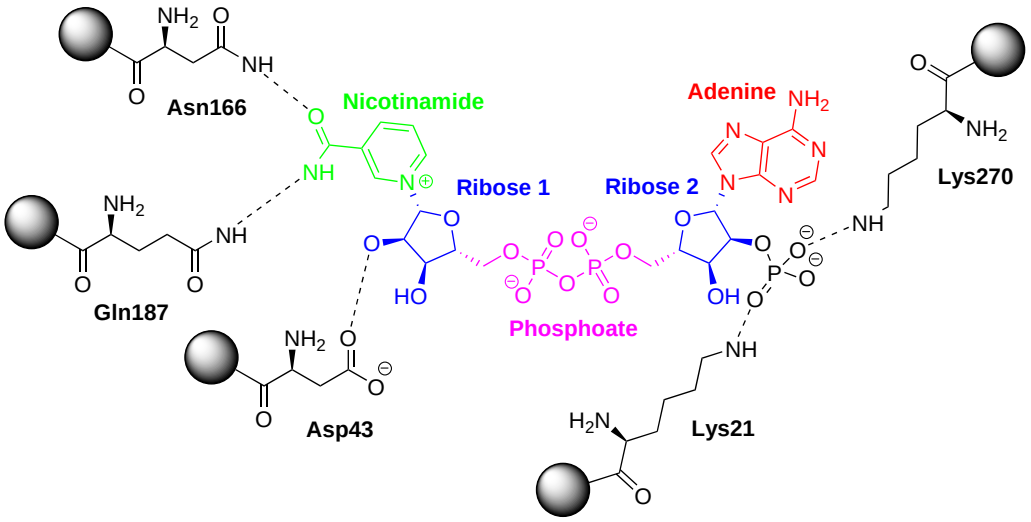

Fig. (6). A 2D diagram for the hydrogen bonding interactions of the cofactor NADP. The chemical of the cofactor NADP is composed of 5 parts: nicotinamide (green), adenine (red), phosphate group (pink) as well as ribose 1 and 2 (blue). The additional phosphate group (black) can form significant hydrogen bonds with Lys21 and Lys270, which was not detected in the cofactor NAD. (For interpretation of the references to color in this figure legend, the reader is referred to the web version of this paper).

specificity, we had to design some mutations which lowered the binding affinity of NADP and changed the cofactor binding site to increase the binding affinity of NAD. According to the previous analyses, we known that the residues in the hydrophilic and hydrophobic pockets played important roles to recognize and position the nicotinamide and adenine moieties which were shared by both NAD and NADP. Thus, it was better to keep these residues, indicating that the desired mutations might be found in the linker channel of the cofactor binding site. Compared with NAD, NADP had an additional phosphate group near the adenine moiety, which could provide additional van der Waals and hydrogen bonding interactions with the neighboring residues. Thus, a possible strategy to lower the binding affinity of NADP was to mutate the residues that had van der Waals or hydrogen bonding interactions with the additional phosphate group in NADP.

As shown in Fig. (**6**), the additional phosphate group in NADP was detected to form hydrogen bonds with Lys21 and Lys270 in the linker channel. These hydrogen bonds were not detected in the binding mode of the cofactor NAD due to lacking the additional phosphate group in Ribose 2 moiety. Thus, mutation in both Lys21 and Lys270 might efficaciously reduce the binding affinity of NADP with few influences on that of NAD. This point was also supported by the previous mutagenesis studies that Lys270 was potential mutation site for altering the cofactor specificity for PsXR [10, 16]. After mutating Lys21 and Lys270 into another 19 amino acids one by one, we found two single mutations K21A and K270N were found to exhibit a significant reversal of the cofactor specificity in PsXR (Table **2**). Compared with the wild-type enzymes, the side-chains of Ala21 and Asn270 in the mutated enzymes were much smaller and shorter, which

Table 2. Experimental Validations of the Specific Activities (U/mg) of the Mutated PsXR

Mutations	Specific Activity	
	NAD	NADP
K21A	2.21 ± 0.15	—
K21R	4.87 ± 0.19	22.3 ± 1.73
K270N	2.15 ± 0.10	—
Wild-type	6.70 ± 0.18	21.0 ± 1.48

broke the significant hydrogen bonds of the additional phosphate group detected in the wild-type enzyme. This was further supported by the fact that the K21R mutation, whose side-chain length was similar with the wild-type, had little influence on the cofactor specific activity.

4. CONCLUSION

We adopted a series of molecular modeling approaches to construct a 3D structural model of PsXR, with an aim of investigating the cofactor specificity of PsXR to solve the intracellular redox imbalance problem during the ethanol production in industry. To validate the structural model, multiple algorithms were utilized to estimate the local and global qualities and stereochemical features; the outcomes indicated that our computational structure of PsXR was quite reliable. Based on the computational structure of PsXR, we also got the favorable binding modes for both NAD and NADP using the flexible docking and molecular dynamics simulation. Our calculations showed that the cofactor binding site in PsXR was composed of 3 major components: a hydrophilic pocket, a hydrophobic pocket and a linker channel between the aforementioned two pockets. The hydrophilic pocket could recognize the nicotinamide moiety of the cofactors through a number of hydrogen bonds, while the hydrophobic pocket functioned to position the adenine moiety of the cofactors by hydrophobic interactions and π-π stacking. The linker channel contained some key residues that had potential abilities to alter the cofactor specificity of PsXR by mutations. Based on the structural comparisons of the binding modes for NAD and NADP, we found that the hydrogen bonds formed by Lys21 and Lys270 only existed in the binding mode of NADP. To alter the major NADP-dependence of PsXR, we mutated these residues into another 19 amino acids, and finally got two single mutations (K21A and K270N). Additional experiments showed that these mutations could significant reverse the cofactor specificity (major NADP-dependence in the wild-type) of PsXR into NAD-dependence. These findings could provide useful insights into the cofactor specificity of PsXR, stimulating novel strategies for re-designing xylose reductase and improving ethanol production in industry.

CONFLICT OF INTEREST

The author(s) confirm that this article content has no conflict of interest.

ACKNOWLEDGEMENTS

This work was supported by the grants from the National High Technology Research and Development Program of China (863 Program, No.2012AA021201), Doctoral Fund of Ministry of Education of China (No.20100093120002), Fundamental Research Funds for the Central Universities (JUSRP111A25), Program of the Science and Technology Support Plan of Jiangsu Province (No.SBE201077545 and SBE201170578), PhD Students Program of Jiangnan University (JUDCF11012), and Priority Academic Program Development of Jiangsu Higher Education Institutions, the 111 Project (No. 111-2-06).

REFERENCES

[1] Kotter, P.; Amore, R.; Hollenberg, C.P.; Ciriacy, M. Isolation and characterization of the Pichia stipitis xylitol dehydrogenase gene, XYL2, and construction of a xylose-utilizing Saccharomyces cerevisiae transformant. *Curr. Genet.*, **1990**, *18*, 493-500.

[2] Takuma, S.; Nakashima, N.; Tantirungkij, M.; Kinoshita, S.; Okada, H.; Seki, T.; Yoshida, T. Isolation of xylose reductase gene of Pichia stipitis and its expression in Saccharomyces cerevisiae. *Appl. Biochem. Biotechnol.*, **1991**, *28-29*, 327-40.

[3] Hyndman, D.; Bauman, D.R.; Heredia, V.V.; Penning, T.M. The aldo-keto reductase superfamily homepage. *Chem. Biol. Interact.*, **2003**, *143-144*, 621-31.

[4] Jez, J.M.; Bennett, M.J.; Schlegel, B.P.; Lewis, M.; Penning, T.M. Comparative anatomy of the aldo-keto reductase superfamily. *Biochem. J.*, **1997**, *326*, 625-36.

[5] Lee, H. The structure and function of yeast xylose (aldose) reductases. *Yeast*, **1998**, *14*, 977-84.

[6] Bedford, J.J.; Bagnasco, S.M.; Kador, P.F.; Harris, H.W., Jr.; Burg, M.B. Characterization and purification of a mammalian osmoregulatory protein, aldose reductase, induced in renal medullary cells by high extracellular NaCl. *J. Biol. Chem.*, **1987**, *262*, 14255-9.

[7] Kador, P.F.; Robison, W.G., Jr.; Kinoshita, J.H. The pharmacology of aldose reductase inhibitors. *Annu. Rev. Pharmacol. Toxicol.*, **1985**, *25*, 691-714.

[8] Toivari, M.H.; Aristidou, A.; Ruohonen, L.; Penttila, M. Conversion of xylose to ethanol by recombinant Saccharomyces cerevisiae: importance of xylulokinase (XKS1) and oxygen availability. *Metab. Eng.*, **2001**, *3*, 236-49.

[9] van Zyl, W.H.; Eliasson, A.; Hobley, T.; Hahn-Hagerdal, B. Xylose utilisation by recombinant strains of Saccharomyces cerevisiae on different carbon sources. *Appl. Microbiol. Biotechnol.*, **1999**, *52*, 829-33.

[10] Watanabe, S.; Abu Saleh, A.; Pack, S.P.; Annaluru, N.; Kodaki, T.; Makino, K. Ethanol production from xylose by recombinant Saccharomyces cerevisiae expressing protein-engineered NADH-preferring xylose reductase from Pichia stipitis. *Microbiology*, **2007**, *153*, 3044-54.

[11] Watanabe, S.; Saleh, A.A.; Pack, S.P.; Annaluru, N.; Kodaki, T.; Makino, K. Ethanol production from xylose by recombinant Saccharomyces cerevisiae expressing protein engineered NADP+-dependent xylitol dehydrogenase. *J. Biotechnol.*, **2007**, *130*, 316-9.

[12] van Maris, A.J.; Winkler, A.A.; Kuyper, M.; de Laat, W.T.; van Dijken, J.P.; Pronk, J.T. Development of efficient xylose fermentation in Saccharomyces cerevisiae: xylose isomerase as a key component. *Adv. Biochem. Eng. Biotechnol.*, **2007**, *108*, 179-204.

[13] Zhang, Y.; Lee, H. Site-directed mutagenesis of the cysteine residues in the Pichia stipitis xylose reductase. *FEMS Microbiol. Lett.*, **1997**, *147*, 227-32.

[14] Kostrzynska, M.; Sopher, C.R.; Lee, H. Mutational analysis of the role of the conserved lysine-270 in the Pichia stipitis xylose reductase. *FEMS Microbiol. Lett.*, **1998**, *159*, 107-12.

[15] Watanabe, S.; Kodaki, T.; Makino, K. Complete reversal of coenzyme specificity of xylitol dehydrogenase and increase of thermostability by the introduction of structural zinc. *J. Biol. Chem.*, **2005**, *280*, 10340-9.

[16] Jeppsson, M.; Bengtsson, O.; Franke, K.; Lee, H.; Hahn-Hagerdal, B.; Gorwa-Grauslund, M.F. The expression of a Pichia stipitis xylose reductase mutant with higher K(M) for NADPH increases ethanol production from xylose in recombinant Saccharomyces cerevisiae. *Biotechnol. Bioeng.*, **2006**, *93*, 665-73.

[17] Petschacher, B.; Nidetzky, B. Altering the coenzyme preference of xylose reductase to favor utilization of NADH enhances ethanol yield from xylose in a metabolically engineered strain of Saccharomyces cerevisiae. *Microb. Cell Fact.*, **2008**, *7*, 9.

[18] Bengtsson, O.; Hahn-Hagerdal, B.; Gorwa-Grauslund, M.F. Xylose reductase from Pichia stipitis with altered coenzyme preference improves ethanolic xylose fermentation by recombinant Saccharomyces cerevisiae. *Biotechnol. Biofuels.*, **2009**, *2*, 9.

[19] Shi, J.; Blundell, T.L.; Mizuguchi, K. FUGUE: sequence-structure homology recognition using environment-specific substitution tables and structure-dependent gap penalties. *J. Mol. Biol.*, **2001**, *310*, 243-57.

[20] Soding, J. Protein homology detection by HMM-HMM comparison. *Bioinformatics*, **2005**, *21*, 951-60.

[21] Wu, S.; Zhang, Y. MUSTER: Improving protein sequence profile-profile alignments by using multiple sources of structure information. *Proteins*, **2008**, *72*, 547-56.

[22] Margelevicius, M.; Venclovas, C. Detection of distant evolutionary relationships between protein families using theory of sequence profile-profile comparison. *BMC Bioinformatics*, **2010**, *11*, 89.

[23] Petschacher, B.; Leitgeb, S.; Kavanagh, K.L.; Wilson, D.K.; Nidetzky, B. The coenzyme specificity of Candida tenuis xylose reductase (AKR2B5) explored by site-directed mutagenesis and X-ray crystallography. *Biochem. J.*, **2005**, *385*, 75-83.

[24] Blundell, T.L.; Sibanda, B.L.; Sternberg, M.J.; Thornton, J.M. Knowledge-based prediction of protein structures and the design of novel molecules. *Nature*, **1987**, *326*, 347-52.

[25] Wu, S.; Skolnick, J.; Zhang, Y. Ab initio modeling of small proteins by iterative TASSER simulations. *BMC Biol.*, **2007**, *5*, 17.

[26] Case, D.A.; Cheatham, T.E.r.; Darden, T.; Gohlke, H.; Luo, R.; Merz, K.M.J.; Onufriev, A.; Simmerling, C.; Wang, B.; Woods, R.J. The Amber biomolecular simulation program. *J. Comput. Chem.*, **2005**, *26*, 1668-88.

[27] Wang, J.F.; Wei, D.Q.; Chen, C.; Li, Y.; Chou, K.C. Molecular modeling of two CYP2C19 SNPs and its implications for personalized drug design. *Protein Pept. Lett.*, **2008**, *15*, 27-32.

[28] Wang, J.F.; Wei, D.Q.; Li, L.; Zheng, S.Y.; Li, Y.X.; Chou, K.C. 3D structure modeling of cytochrome P450 2C19 and its implication for personalized drug design. *Biochem. Biophys. Res. Commun.*, **2007**, *355*, 513-9. Erratum in: Biochem. Biphys. Res. Commun., 2007, 357, 330. Biochem. Biophys. Res. Commun., 2009, 384, 399.

[29] Li, J.; Wei, D.Q.; Wang, J.F.; Li, Y.X. A negative cooperativity mechanism of human CYP2E1 inferred from molecular dynamics simulations and free energy calculations. *J. Chem. Inf. Model.*, **2011**, *51*, 3217-25.

[30] Wang, J.F.; Chou, K.C. Insights into the mutation-induced HHH syndrome from modeling human mitochondrial ornithine transporter-1. *PLoS One*, **2012**, *7*, e31048.

[31] Chen, Q.; Zhang, T.; Wang, J.F.; Wei, D.Q. Advances in human cytochrome p450 and personalized medicine. *Curr. Drug Metab.*, **2010**, *12*, 436-44.

[32] Wang, J.F.; Chou, K.C. Molecular modeling of cytochrome P450 and drug metabolism. *Curr. Drug Metab.*, **2010**, *11*, 342-6.

[33] Wang, Y.; Wu, X.L.; Wei, D.Q.; Li, Y.X.; Wang, J.F. Autoinhibitory mechanism for the mutation-induced impaired FGF9 signaling. *J. Chem. Inf. Model.*, **2012**, *52*, 2422-9.

[34] Wang, J.F.; Chou, K.C. Insight into the molecular switch mechanism of human Rab5a from molecular dynamics simulations. *Biochem. Biophys. Res. Commun.*, **2009**, *390*, 608-12.

[35] Lian, P.; Wei, D.Q.; Wang, J.F.; Chou, K.C. An allosteric mechanism inferred from molecular dynamics simulations on phospholamban pentamer in lipid membranes. *PLoS One*, **2011**, *6*, e18587.

[36] Benkert, P.; Tosatto, S.C.; Schomburg, D. QMEAN: A comprehensive scoring function for model quality assessment. *Proteins.*, **2008**, *71*, 261-77.

[37] Zhou, H.; Zhou, Y. Distance-scaled, finite ideal-gas reference state improves structure-derived potentials of mean force for structure selection and stability prediction. *Protein Sci.*, **2002**, *11*, 2714-26.

[38] Laskowski, R.A.; Rullmannn, J.A.; MacArthur, M.W.; Kaptein, R.; Thornton, J.M. AQUA and PROCHECK-NMR: programs for checking the quality of protein structures solved by NMR. *J. Biomol. NMR*, **1996**, *8*, 477-86.

[39] Chou, K.C.; Scheraga, H.A. Origin of the right-handed twist of beta-sheets of poly-L-valine chains. *Proc. Natl. Acad. Sci. USA*, **1982**, *79*, 7047-51.

Received: November 07, 2012 Revised: March 07, 2013 Accepted: March 07, 2013